Discrimination of local radiative and nonradiative recombination processes in an InGaN/GaN single-quantum-well structure by a time-resolved multimode scanning near-field optical microscopy

AUTHOR(S):

Kaneta, A; Mutoh, T; Kawakami, Y; Fujita, S; Marutsuki, G; Narukawa, Y; Mukai, T

CITATION:

Kaneta, A ...[et al]. Discrimination of local radiative and nonradiative recombination processes in an InGaN/GaN single-quantum-well structure by a time-resolved multimode scanning near-field optical microscopy. APPLIED PHYSICS LETTERS 2003, 83(17): 3462-3464

ISSUE DATE:

2003-10-27

URL:

http://hdl.handle.net/2433/50566

Discrimination of local radiative and nonradiative recombination processes in an InGaN/GaN single-quantum-well structure by a time-resolved multimode scanning near-field optical microscopy

Akio Kaneta,[a] Takashi Mutoh, Yoichi Kawakami, and Shigeo Fujita
Department of Electronic Science and Engineering, Kyoto University, Yoshida-honmachi, Sakyo-ku, Kyoto, 606-8501 Japan

Giichi Marutsuki, Yukio Narukawa, and Takashi Mukai
Nichia Corporation, 491 Oka, Kaminaka, Anan, Tokushima, 774-8601 Japan

(Received 12 May 2003; accepted 28 August 2003)

Precise identification of recombination dynamics based on local, radiative, and nonradiative recombination has been achieved at room temperature in a blue-light-emitting $In_xGa_{1-x}N/GaN$ single-quantum-well structure by comparing the photoluminescence (PL) spectra taken by illumination-collection mode (I-C mode) and those by illumination mode (I-mode) in scanning near-field microscopy. The PL data mapped with PL lifetimes, as well as with PL spectra, revealed that the probed area could be classified into four different regions whose dominating processes are (1) radiative recombination within a probing aperture, (2) nonradiative recombination within an aperture, (3) diffusion of photogenerated excitons/carriers out of an aperture resulting in localized luminescence, and (4) the same diffusion process as (3), but resulting in nonradiative recombination. © *2003 American Institute of Physics.* [DOI: 10.1063/1.1620677]

Very bright blue-light-emitting diodes (LEDs) have been developed recently, since the breakthrough of growth technology of $In_xGa_{1-x}N/GaN/Al_yGa_{1-y}N$ heterostructures.[1–3] In spite of high threading dislocation density (10^8–10^{10} cm^{-2}) in GaN epilayers grown on sapphire substrates, an external quantum efficiency (η_{ext}) of about 20% is now commercially available emitting in a spectral range from violet (400 nm) to blue (465 nm).[4] Two models have been reported so far to elucidate the emission phenomena occurring in the GaN epilayers. The first explains that incorporation of In to Ga site is an effective process for suppressing nonradiative recombination centers associated with point defects.[5] Another one concerns the effects of exciton localization that is caused by compositional fluctuation of In; the pathways of nonradiative recombination centers are hindered once excitons are captured at potential minima.[6,7]

We have recently reported about the spatial distribution of photoluminescence (PL) in an $In_xGa_{1-x}N$ single-quantum-well (SQW) in a study employing scanning near-field optical microscopy (SNOM) under illumination-collection mode (I-C mode) at 18 K.[8]

In I-C mode, the photoexcitation and the PL probing are accessed through the same optical aperture at the apex of the fiber probe; thus, the spatial resolution is limited only by its size.[9] In our specific case, we could achieve a resolution of about 30 nm. On the contrary, the conventional illumination mode (I-mode), where the photoexcitation is given through the fiber tip and the PL signal is collected by objective lens in far-field configuration, is characterized by lower optical resolution. The observed spatial resolution depends not only by the optical aperture, but also by other factors. For example, higher carrier mobility in the vicinity of the tip will induce radiative recombination processes also in regions not directly under the probe. This signal will be not detectable in I-C mode, but visible by a far-field detector of an I-mode configuration. However, a disadvantage of I-C mode is that it is difficult to assign the observation of weak PL intensity to a nonradiative recombination process, or to a diffusion of photo-generated carriers outside the area of detection of the fiber probe. This is critical for the measurement at room temperature because the former process cannot be neglected, unlike at cryogenic temperatures. Focusing on these optical configuration problems, and understanding the importance to collect different signal simultaneously, we set up a SNOM apparatus able to operate simultaneously in multiple modes, I-mode, and I-C mode, and designed to probe time-resolved PL (TRPL) spectra in both modes. The multiple measurements taken in this way allowed us to map the PL signal at

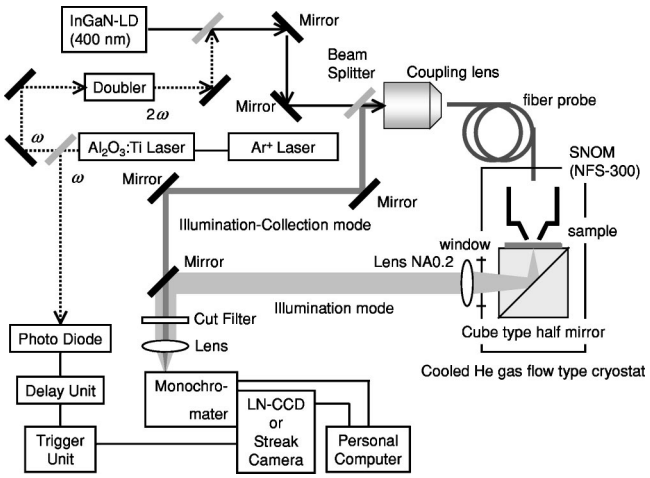

FIG. 1. Schematic of the experimental setup. The system is able to work simultaneously in I-C mode, I-mode, and to perform TRPL analysis.

[a]Electronic mail: kaneta@fujita.kuee.kyoto-u.ac.jp

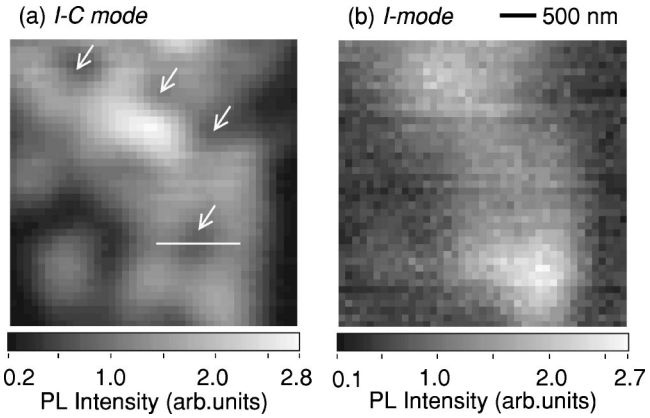

FIG. 2. Near-field PL intensity images taken under I-C mode (a) and I-mode (b) probed with double tapered fiber (aperture size is 200 nm in diameter) at RT. The excitation power density is 2.5 kW/cm^2 under cw condition. The scanning area is 4 μm×4 μm with probing step of 100 nm. The PL intensity is normalized to unity.

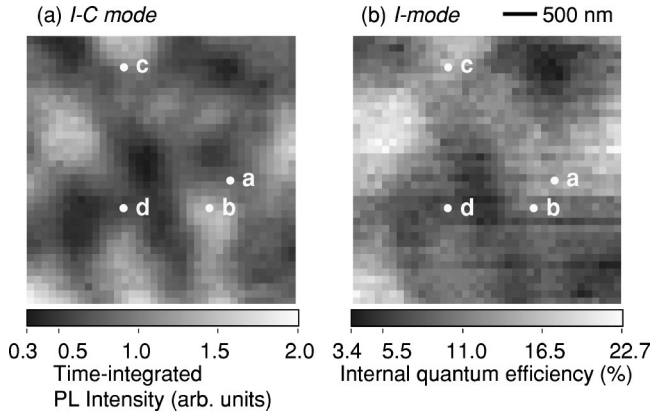

FIG. 4. Time-integrated near-field PL intensity images taken under I-C mode (a) and I-mode (b) probed with single tapered fiber (pure SiO_2, aperture size is 200 nm in diameter) at RT. The excitation power density is 5.5 μJ/cm^2 under pulsed condition. The scanning area is 3.7 μm×3.7 μm with the probing step of 100 nm. The PL intensity is normalized to unity.

high resolution and we could clearly discriminate radiative and nonradiative processes in $In_xGa_{1-x}N$-based semiconductors.

The sample is composed of a sapphire (0002) substrate, a 4-μm-thick undoped GaN, a 3-nm-thick $In_xGa_{1-x}N$-SQW active layer (x = about 0.2) and a 5-nm-thick undoped GaN layer. Macroscopic PL peak is located at about 460 nm at RT. A schematic experimental setup is shown in Fig. 1. The measurements were performed with NFS-300 near-field spectrometer developed at JASCO Corp. The tapered structure of fiber probe is fabricated by etching using hydrofluoric-buffered solution.[9] An $In_xGa_{1-x}N$-based laser diode emitting at 400 nm (developed at Nichia Corp.) was used as the excitation source of cw PL. The cw PL signal was introduced into a 50-cm monochromator, and then detected by a liquid-nitrogen-cooled CCD detector (Roper Scientific, Spec-10:100B/LN). A frequency-doubled, mode-locked Al_2O_3:Ti laser emitting at 400 nm with the pulse width of 1.5 ps was used as an excitation source. A streak camera (Hamamatsu Photonics, C5680) was used as a detector. The measurements were performed at room temperature.

Figure 2 shows spatial distribution of PL peak intensity under I-C mode (a) and I-mode (b) taken in the same scanning area. Concerning the I-C mode measurement, it was found that relative PL intensity fluctuates from 0.2 to 2.8, consisting of island like structures within the range of approximately 0.3-1 μm. On the other hand, in I-mode measurement, relative PL intensity fluctuates from 0.1 to 2.7, a value larger than that of I-C mode. Our SNOM apparatus regulates the sample–probe separation with a shear force (SF) system,[10] SF signal assessed *in situ* during the SNOM measurements shows that the root mean square of surface roughness is as small as 3.1 nm, and that there is no correlation with PL intensity signal within the scanning area of 4 μm×4 μm. In Figs. 2(a) and 2(b), we show the I-C mode and I-mode maps obtained simultaneously on a certain area of our sample. The two images present quite interesting differences. We can notice the presence of weak PL intensity domains in I-C mode (indicated by the arrows) that appear as high PL intensity in I-mode. Other regions appears to remain unchanged if observed in the two modes. This behavior can be explained as follows. In the case of domains that appear of weak PL intensity in I-C mode and turn out as high PL intensity in I-mode, we believe that the carrier and/or exciton that are photogenerated directly under the optical aperture of the probe, are diffused and localized to out of the I-C mode probing area, but they remain in the range of the far-field I-mode detector.

In the other case, the photogenerated carriers and/or excitons do not migrate further than the I-C mode probing region, they are presumably captured at nonradiative recombination centers, origin of which are related to microscopic dislocations and/or to nanoscopic point defects. A cross-sectional profile of PL intensity along the white line in Fig. 2(a) is plotted in Fig. 3. The full width at half-maximum of a Gaussian fitting result of this profile is 550 nm; therefore, the diffusion length to radiative recombination center is at least

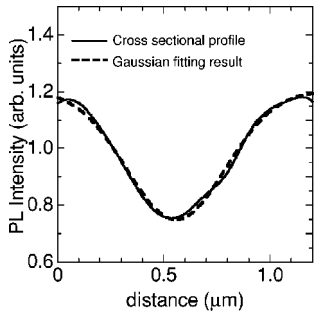

FIG. 3. Cross-sectional profile of PL intensity along the white bar in Fig. 2(a).

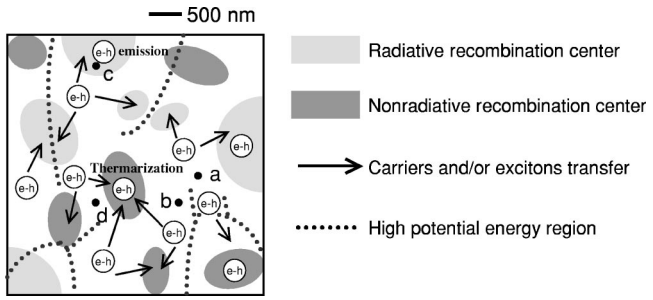

FIG. 5. Schematics of the different carrier dynamics as observed in Fig. 4 with its four studied points a, b, c, and d.

TABLE I. We classified the carrier dynamics observation of Fig. 4 in four different behavior classes, each represented by the four points (a,b,c, and d) in this table.

Position	$I_{\text{I-C mode}}$	$I_{\text{I-mode}}$	η_{int} (%)	$\tau_{\text{PL-IC}}$ (ns)	$\tau_{\text{PL-I}}$ (ns)	$\tau_{\text{tr-out}}$ (ns)	τ_{rad} (ns)	$\tau_{\text{non-rad}}$ (ns)
a	Weak	Strong	21.1	0.541	1.553	0.83	7.35	1.97
b	Strong	Weak	15.0	0.580	0.673	4.18	4.49	0.79
c	Strong	Strong	22.6	0.564	0.568	87.1	2.50	0.73
d	Weak	Weak	9.0	0.552	0.677	3.00	7.44	0.74

275 nm in this area. It is interesting to note that the similar value is reported by Cherns *et al.* as the diffusion length in InGaN-based quantum structures using cathodoluminescence spectroscopy technique.[11]

Figures 4(a) and 4(b) show the time-integrated PL-intensity mapped in I-C mode and I-mode, respectively. TRPL was detected at four different positions that are indicated with the letters (a)-(d). These positions were selected as representative of four different behaviors: (a) relatively weak PL intensity in I-C mode while stronger PL intensity in I-mode; (b) opposite situation to the case of (a); (c) relatively strong PL intensity in both modes; and (d) relatively weak PL intensity in both modes. It was found that the PL lifetimes (τ_{PL}) under I-C mode are always shorter than those in I-mode. The difference is significant for the data at (a), where τ_{PL} values are 0.541 and 1.553 ns, for I-C mode and I-mode, respectively. The PL lifetime in I-C mode ($\tau_{\text{PL-IC}}$) is $1/\tau_{\text{PL-IC}}=1/\tau_{\text{rad}}+1/\tau_{\text{nonrad}}+1/\tau_{\text{tr-out}}$, where τ_{rad} and τ_{nonrad} are radiative and nonradiative lifetimes, respectively, and $\tau_{\text{tr-out}}$ represents the lifetime of carrier transfer from the area directly under the tip aperture (within the I-C mode probing range, I-C mode and I-mode detection are both possible) and a region external to it (in this case, only I-mode detection is possible). Since a PL signal is detected in far-field configuration under I-mode, the term of $1/\tau_{\text{tr-out}}$ can be neglected; the PL lifetime under I-mode ($\tau_{\text{PL-I}}$) is expressed by $1/\tau_{\text{PL-I}}=1/\tau_{\text{rad}}+1/\tau_{\text{nonrad}}$. PL intensity mapped under I-mode [Fig. 4(b)] represent the spatial distribution of internal quantum efficiency. According to the temperature dependence of macroscopic PL measurements, it was found that the internal quantum efficiency of this sample is nearly unity (more than 90%) at temperatures less than 50 K.[12] Consequently, the distribution of PL intensities from 0.1 to 2.7 at RT corresponds to η_{int} values ranging from 3.4% to 22.7%. Since the η_{int} value is expressed by $\eta_{\text{int}}=\tau_{\text{nonrad}}/(\tau_{\text{rad}}+\tau_{\text{nonrad}})$, all recombination lifetimes can be calculated using the experimental data as shown in Table I.[13] It is evident that the shorter lifetime of $\tau_{\text{PL-IC}}$ probed at position (a) is due to a small $\tau_{\text{tr-out}}=0.83$ ns term. This transfer process is probably caused by exciton/carrier localization centers that are local potential minima distributed in the proximity of the tip, but external of the I-C mode probing range. This idea is confirmed by examining the time integration of the PL peaks, in the case of position (a) the time integrated peak is located at 461.9 nm (2.683 eV) under I-C mode, while it is at 464.2 nm (2.670 eV) under I-mode.

In the point indicated with (b), relatively weak PL intensity in I-mode is caused by a transfer process to nonradiative recombination centers distributed in the region external to the I-C mode probing, as it is indicated by the small $\tau_{\text{nonrad}}=0.79$ ns. Concerning the point in (c), the strong PL intensities in both modes are due to radiative recombinations that mainly take place within the aperture, as shown by a large value of $\tau_{\text{tr-out}}=87.1$ ns. Moreover, in the position (d), a weak PL intensity in both modes is due by large density of nonradiative recombination centers distributed within and outside of the aperture range.

Based on the dynamics just described, the transfer, radiative, and nonradiative processes taking place are represented in the scheme of Fig. 5. Radiative and nonradiative recombination centers are present all over the sample. However, their densities is inhomogeneous. Higher density of radiative recombination domains act as attractive centers for photogenerated excitons/carriers. Potential energy was estimated by the mapping of PL peak; in Fig. 5, the dotted lines represent regions where the potential energy is higher. These high-energy lines form a potential ridge that presumably would suppress the carrier/exciton diffusion, creating the carrier dynamic we observed.

The authors would like to thank Dr. Funato and Dr. Micheletto for valuable comments and discussion. We are also grateful to Mr. Narita at JASCO Corp. for contributing the setup of SNOM. This work was partly supported by the Kyoto University-Venture Business Laboratory Project, the Mizuho Foundation for the Promotion of Sciences, the 21st Century COE Program (No. 14213201), and by a Grant-in-Aid for the special area research project of Photonics based on wavelength integration and manipulation from the Ministry of Education, Science, Sports and Culture, Japan.

[1] S. Nakamura, M. Senoh, N. Iwasa, and S. Nagahama, Jpn. J. Appl. Phys. **34**, L797 (1995).
[2] S. Nakamura, M. Senoh, N. Iwasa, S. Nagahama, T. Yamada, and T. Mukai, Jpn. J. Appl. Phys. **34**, L1332 (1995).
[3] T. Mukai, H. Narimatsu, and S. Nakamura, Jpn. J. Appl. Phys. **37**, L479 (1998).
[4] M. Yamada, Y. Narukawa, and T. Mukai, Jpn. J. Appl. Phys. **41**, L246 (2002).
[5] Y. Narukawa, S. Saijou, Y. Kawakami, Sg. Fujita, T. Mukai, and S. Nakamura, Appl. Phys. Lett. **74**, 558 (1999).
[6] S. Chichibu, T. Azuhata, T. Sota, and S. Nakamura, Appl. Phys. Lett. **69**, 4188 (1996).
[7] Y. Narukawa, Y. Kawakami, M. Funato, Sz. Fujita, Sg. Fujita, and S. Nakamura, Appl. Phys. Lett. **70**, 981 (1997).
[8] A. Kaneta, K. Okamoto, Y. Kawakami, Sg. Fujita, G. Marutsuki, Y. Narukawa, and T. Mukai, Appl. Phys. Lett. **81**, 4353 (2002).
[9] T. Saiki, K. Nishi, and M. Ohtsu, Jpn. J. Appl. Phys. **37**, 1638 (1998).
[10] E. Betzig, P. L. Finn, and J. S. Weiner, Appl. Phys. Lett. **60**, 2484 (1992).
[11] D. Cherns, S. J. Heniey, and F. A. Ponce, Appl. Phys. Lett. **78**, 2691 (2001).
[12] R. C. Miller, D. A. Kleinman, W. A. Nordland, Jr., and A. C. Gossard, Phys. Rev. B **22**, 863 (1980).
[13] The first-order assumption used in this calculation, where radiative lifetimes as well as nonradiative lifetimes in illumination mode are same as those in illumination collection mode. More detailed analysis taking into account the difference in radiative/nonradiative lifetimes are in progress.